Friedrich Miescher Institute
for Biomedical Research

Master Thesis

Single-molecule imaging of mRNA to study translational regulation

Author:
Bastian Th. Eichenberger
Supervisor:
Jeffrey A. Chao and Susan E. Mango

UNIVERSITY OF BASEL
Basel, Switzerland

A thesis submitted in fulfillment of the requirements for the degree of Master of Science in Molecular Biology.

May 2020

Abstract

Stress granules are cytoplasmic, membrane-less organelles containing a plethora of proteins involved in translation initiation and repression. They are exclusively formed in stress conditions. This study attempts to better understand the role of stress granules by focussing on a core protein component: G3BP1. By tethering G3BP1 to specific mRNAs, various single-molecule imaging tools were used to investigate G3BP1's effect on translation and stability. G3BP1 appears to increase reporter protein production by a significant margin by mRNA stabilization. Lastly, a new translation site imaging tool is presented which can be used in future studies to address the many unanswered questions.

Keywords: Stress granules, G3BP1, SunTag Imaging, TREAT, Luciferase assay, mRNA Tethering.

Acknowledgments

First and foremost, I would like to thank Jeff for making this project possible and keeping me (at least somewhat) on the right track and encouraging me to dive deeper into coding. Next, I can count myself lucky for having an awesome supervisor in Daniel who remained critical and always helpful if questions arose. Regarding questions..., I had a few. And without Pratik and Franka many of those would have remained unanswered. They gave me helpful comments on improving this very document and contributed to a pleasant lab atmosphere. In a rather busy time, Varun was friendly enough to clone the smGFP plasmid which made me have more time to focus on other important things at hand. Finally, a big thank you to Susan for accepting in being the official part of the university and grading this thesis.

Contents

1 Introduction

1.1 mRNA Life Cycle

Transcription is the first step in gene expression in which a premature RNA molecule is made from a gene's DNA template. In eukaryotes, splicing, adding a 5' cap and poly-A-tail, as well as binding of cap- and RNA-binding proteins yields mature messenger RNAs (mRNAs). As transcription and translation are compartmentally separated, these mRNAs are then typically exported through nuclear pore complexes, which perforate the nuclear envelope. Once in the cytoplasm, the acquired protein coat determines the fate of the mRNA [1]. One of these fates is translation to produce proteins. This process involves polysome (mRNA bound ribosome clusters) assembly and messenger ribonucleoprotein complex (mRNP) remodeling and can occur immediately or delayed, such as in the case of various developmental transcripts. If a protein no longer needs to be produced, polysomes get disassembled and mRNAs might be deadenylated. mRNAs are now usually degraded or stored until internal or external signals call for their renewed translation. Subsets of these mRNAs can be packaged into RNA granules (Figure 1.1A). RNA granules are cytoplasmic, membrane-less aggregates containing various proteins involved in translation initiation and repression (reviewed in [2]).

Stress granules (SGs) are a prominent type of RNA granules that exclusively form under stress. Cellular stress arrives from various external or internal fac-

tors and can trigger the integrated stress response pathway. Typical extrinsic factors range from starvation, infection, hypoxia, the presence of oxidants, and many more. The largest intrinsic factor is endoplasmic reticulum (ER) stress through the accumulation of unfolded or misfolded proteins. All of these activations converge to the phosphorylation of the α subunit on eukaryotic trans-

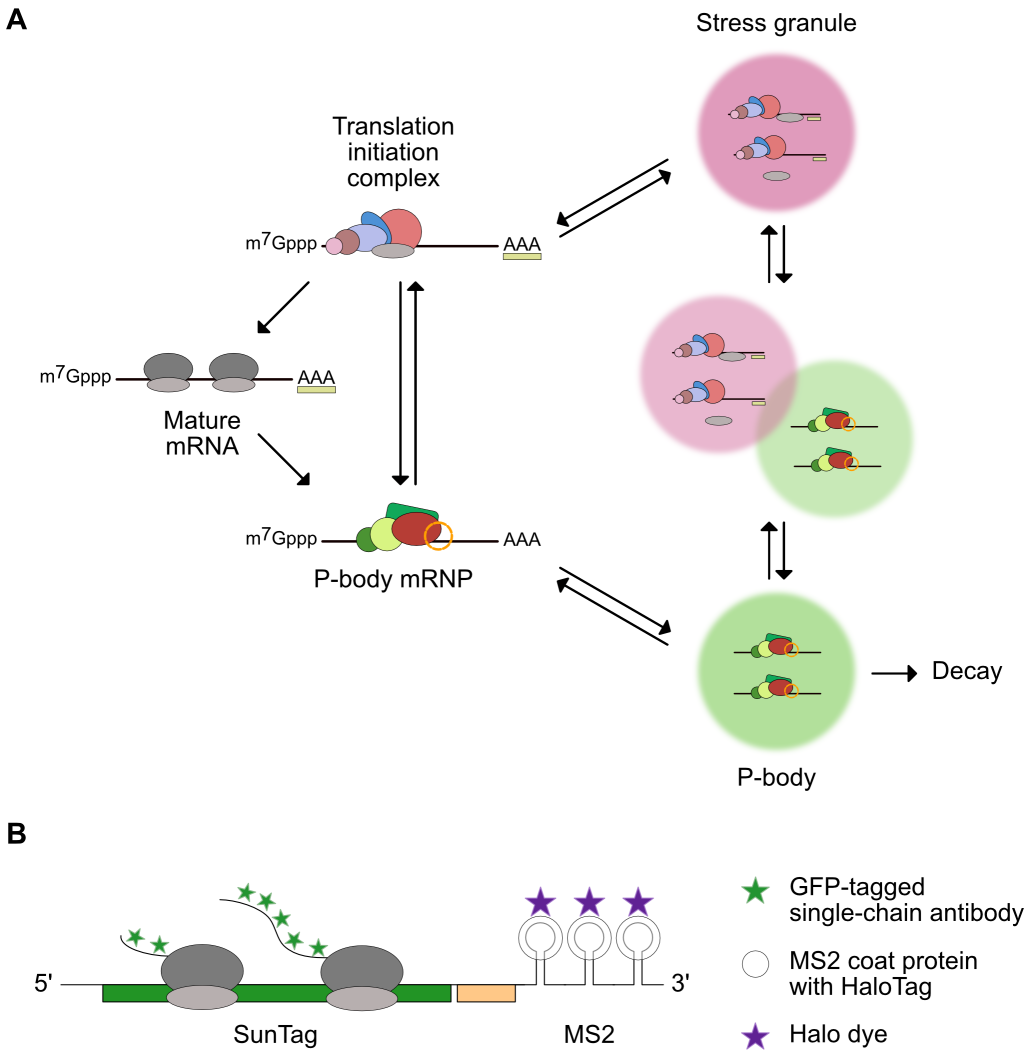

Figure 1.1: (Continued on the following page.)

Figure 1.1: mRNA life cycle and translation site imaging. (A) Overview of a mature, translating mRNAs life cycle. Protein components of the translation initiation complex together with their bound mRNAs can aggregate into membrane-less organelles termed stress granules. A similar type of RNA granule, the P-bodies, have been associated with mRNA decay and a different set of proteins. Both granules can interact and possibly exchange components. (B) Schematic description of SunTag imaging to visualize and quantify translational activity on single-molecule level.

lation initiation factor 2 (eIF2α). This phosphorylation deactivates eIF2α and inhibits global protein synthesis which inturn can lead to an up-regulation of stress-response genes (reviewed in [3]). Multiple immunofluorescence-based studies have shown that SGs showed an enrichment in initiation factors including eIF2 but not for other translation-related machinery components such as the 60S ribosomal subunit [4]. Some proteins found in SGs such as the proteins T-cell intracellular antigen-1 (TIA-1) [5] and Ras GTPase-Activating Protein-Binding Protein 1 (G3BP1) [6] have been found to induce SG formation upon overexpression. The exact nature of SG formation is unknown but various mechanisms from prion-like assembly [7, 8], maturation of mRNA Processing Bodies (P-bodies) (described below) [9], and microtubule involvement have been proposed [10]. While SG formation seems to be a conserved phenomenon throughout eukaryotes, their function also remains unclear. Observations suggest an involvement of SGs in mRNA stability and repression (reviewed in [11]). This, in conjunction with their enrichment in initiation factors, leads to the assumption that SGs exclusively contain translationally repressed mRNAs (reviewed in [12]). However, recent findings have reported that some SG-localized mRNAs can still be translated [13].

A different type of RNA granules, the P-bodies, were originally described as mouse XRN1p (a highly conserved 5'-3' exonuclease) foci in the cytoplasm [14]. P-bodies, unlike SGs, are present in unstressed physiology. However, stress can further increase their formation (reviewed in [15]). Contrasting SGs,

they contain non-overlapping protein components including multiple nucleases that have made them a proposed site of mRNA decay [16].

1.2 Translation Site Imaging

To better understand the translational dynamics of single transcripts, a recent method has emerged. The stellar explosion SUperNova (SunTag) imaging approach allows for live-cell imaging-based analysis to visualize and quantify translation sites [17]. The SunTag system relies on three core components: a reporter RNA containing a SunTag cassette and MS2 stem-loops, a green fluorescent protein (GFP)-tagged single-chain antibody (scAB) against GCN4, and an MS2 coat protein fused to a HaloTag (Figure 1.1B).

The MS2 system has been widely adopted to tag and visualize specific mRNAs. MS2 stem-loops serve as structural motifs and are naturally recognized by the MS2 bacteriophage capsid RNA-binding protein MS2 (MCP) (reviewed in [18]). Typical MS2 tagging involves the visualization of single mRNAs encoding an array MS2 stem-loops by an MCP-GFP fusion. Multiple MS2 stem-loops are used to increase the local concentration of MCP bound fluorescent molecules allowing for significant signal amplification. Previous studies have used this method to investigate mRNA metabolism by tethering mRNAs to membranes [19], to proteins [20], or to themselves as shown in a recent optogenetic clustering approach [21].

Currently available standard SunTag cassettes consist of 24 GCN4 epitope repeats that, upon translation and exposure of the GCN4 epitopes, can be recognized and bound by the co-expressed GFP-tagged scAB. As translation continues, more epitopes get synthesized allowing more scABs to bind. This increases the local concentration and thereby brightens the fluorescent signal. Once translation is terminated, SunTag peptides together with attached scABs are released from the mRNA and rapidly degraded causing a decrease in signal intensity. Degradation is increased due to an FKBP tag that is located

C-terminal of the SunTag cassette and that targets the newly formed protein for proteasomal degradation [22]. The MS2 coat protein-HaloTag fusion in conjunction with a soluble Halo dye is used to visualize the MS2 stem loops on the reporter RNA. Taken together, the system allows for accurate tracking of single RNAs and simultaneous brightness-inferred translational quantification.

This study focusses on the understanding of how SGs form and how they function. Using modified components of the SunTag imaging system, a core SG protein, G3BP1 is used as the main antagonist to provide interesting insights into the unknown world of SGs. Lastly, an improvement to the existing SunTag system is proposed.

2 Methods

2.1 Key Resources

Table 2.1: Antibodies

Reagent or Resource	Source	Identifier
Alexa Fluor 647	Abcam	ab150075
TIA-1	Abcam	ab40693

Table 2.2: Experimental Models: Cell lines

Reagent or Resource	Source	Identifier
Hela 11ht	Weidenfeld et al., 2009 [23]	N/A
Hela 11ht + scAB-GFP + Renilla-MS2	This study	N/A
Hela 11ht + scAB-GFP + smGCN4-Renilla-MS2	This study	N/A
Hela 11ht + scAB-GFP + SunTag-Renilla-MS2	This study	N/A
Hela 11ht + TREAT	This study	N/A

Table 2.3: Chemicals and Peptides

Reagent or Resource	Source	Identifier
Amino-11-ddUTP	Lumiprobe	15040
Atto 647N NHS ester	Sigma-Aldrich	AD 647N-31
Bovine serum albumin	Sigma-Aldrich	A2153-50G
Dextran sulfate	Sigma	D6001-50G
Doxycycline	Sigma	D3891-1G
FluoroBrite DMEM	Life Technologies	A1896703
Formamide (deionized)	Chemicon	S4117
Ganciclovir	Sigma-Aldrich	G2536-100MG
JF585 HaloTag ligand	Grimm et al., 2015, 2017 [24, 25]	N/A
Lipofectamine 2000	Invitrogen	11668019
Opti-MEM^{TM}	Gibco	31985070
Paraformaldehyde 20% (aqueous)	Electron Microscopy Sciences	15713
ProLong Gold Antifade Mountant	Molecular Probes, Life Technologies	P36935
Puromycin	Invivogen	ant-pr-1
Sodium Arsenite solution	Sigma	35000-1L-R

Table 2.4: Critical Commercial Assays

Reagent or Resource	Source	Identifier

continues on next page

Reagent or Resource	Source	Identifier
Bradford Protein Assay	Biorad	5000006
Renilla Luciferase Assay System	Promega	E2810

Table 2.5: Oligonucleotides

Reagent or Resource	Source	Identifier
Oligodeoxyribonucleotides and primers are listed in Appendix A.	N/A	N/A

Table 2.6: Recombinant DNA

Reagent or Resource	Source	Identifier
G3BP1-GFP-GFP	Wilbertz et al., 2019 [26]	Addgene #119950
NLS-stdMCP-stdHalo	Voigt et al., 2017 [27]	Addgene #104999
NLS-stdMCP-stdHalo-G3BP1	This Study	N/A
NLS-stdMCP-stdHalo-Rh1	This Study	N/A
pCAGGS-FLPe-IRESpuro	Beard et al., 2006 [28]	Addgene #20733
Renilla-MS2v5	This Study	N/A
scAB-GFP	Voigt et al., 2017 [27]	Addgene #104998

continues on next page

Reagent or Resource	**Source**	**Identifier**
smGCN4-Renilla-MS2v5	This study	N/A
SunTag-Renilla-MS2v5	Wilbertz et al., 2019 [26]	Addgene #119945
SunTag-Renilla-PP7-MS2v4	Horvathova et al., 2017 [29]	N/A

Table 2.7: Critical Equipment

Reagent or Resource	**Source**	**Identifier**
405 iBeam Smart	Toptica Photonics	N/A
488 iBeam Smart	Toptica Photonics	N/A
561 Cobolt Jive	Cobolt	N/A
639 iBeam Smart	Toptica Photonics	N/A
96-Well White Polystyrene Microplates	Costar	07-200-589
CFI Plan Apochromat Lambda 100x Oil/1.45 Objective	Nikon	N/A
CSU-W1 Confocal Scanner Unit	Yokogawa	N/A
Glass Coverslips	Paul Marienfeld GmbH	117580
iXon-Ultra-888 EMCCD Cameras	Andor	N/A
Mithras Multimode Microplate Reader LB 940	Berthold	38099

continues on next page

Reagent or Resource	Source	Identifier
MS-2000 Motorized Stage	Applied Scientific Instrumentation	N/A
TetraSpeck™ Fluorescent Microspheres Size Kit	Thermo Fisher Scientific	T14792
Ti2-E Eclipse Inverted Microscope	Nikon	N/A
VS-Homogenizer	Visitron Systems GmbH	N/A

Table 2.8: Software and Algorithms

Reagent or Resource	Source	Identifier
Affinity Designer 1.8.2	Serif (Europe) Ltd	`affinity.serif.com/designer/`
Benchling 2020	Benchling	`benchling.com`
Fiji 2.0.0-rc-69/1.52p	Schindelin et al., 2012 [30]	`fiji.sc`
Fluffy 0.2.2	Eichenberger, 2020 [31]	`github.com/BBQuercus/fluffy`
KNIME 3.7.2	Berthold et al., 2009 [32]	`knime.com/knime-analytics-platform`
PyMOL 2.3.3	Schrodinger LLC.	`pymol.org`
Python 3.7.4	Python Software Foundation	`python.org`
TrackMate v5.2.0	Tinevez et al., 2017 [33]	`imagej.net/TrackMate`

continues on next page

Reagent or Resource	Source	Identifier
VisiView 4.4.0	Visitron Systems GmbH	visitron.de/products/visiviewr-software

2.2 Method Details

Cell lines and culture details

The previously described HeLa-11ht cell line [23] was used for this study. The integrated Flp-RMCE (recombinase-mediated cassette exchange) site allows for controlled, single-copy, genomic integration of a target gene. In addition, to induce inserted target genes reversibly with doxycycline, cells are expressing a reverse tetracycline controlled transactivator (rtTA2S-M2). Dulbecco's Modified Eagle Medium (DMEM) containing 4.5 g/l glucose, 100 U/ml Penicillin, 100 µg/ml Streptomycin, 4 mM L-Glutamine, and 10% v/v Fetal Bovine Serum (FBS) was used to culture HeLa cells. Cells were maintained at 37°C with 5% CO_2. Transient transfections were performed with Lipofectamine 2000 transfection reagent (Invitrogen) with Opti-MEM reduced serum medium (Gibco) according to manufacturer's instructions but scaled down to 0.5 µg plasmid DNA and 2 µl Lipofectamine 2000 per 1 ml growth medium.

Plasmid construction

To generate the G3BP1 coat protein fusion, the genomic sequence encoding the full-length G3BP1 Isoform 1 (Q13283-1) was inserted in-frame, downstream of the HaloTag sequence. A 33 nt linker sequence was kept between HaloTag and G3BP1 to ensure steric movement. Assembly was performed by PCR amplification of G3BP1 and the MCP-Halo-linker backbone, followed by Gibson cloning [34]. The resulting construct contains a constitutive UbiC promoter, SV40 NLS (nuclear localization signal), stdMCP (MS2 coat protein), HaloTag, 33 nt linker sequence, G3BP1 with a stop codon, and a Woodchuck

Hepatitis Virus Posttranscriptional Regulatory Element (WPRE) improving expression in lentiviral transfection (Figure B.1).

The smGCN4 reporter sequence containing GCN4 epitopes was synthesized into a pUC57-Kan expression vector. Assembly was performed by PCR amplification of smGCN4 and the *Renilla*-MS2v5 backbone followed by Gibson cloning. The resulting plasmid contains a Tet-CMV (cytomegalovirus) promoter followed by smGCN4, *Renilla* luciferase, FKBP domain with a stop codon, MS2v5 stem-loop cassette (24x), CTE (constitutive transport element, and SV40 polyA tail (Figure B.2).

Reporter cell line generation

A day before selection, HeLa cells were seeded into a 6-well plate. The targeting plasmid containing the reporter (2 µg) and pCAGGS-FLPe-IRESpuro plasmid (2 µg) were transfected using Lipofectamine 2000 (Invitrogen) according to manufacturers' protocol [28]. On the next day, cells were preselected with 5 µl/ml puromycin (Invivogen). Two days later, the puromycin-containing medium was removed and replaced with fresh growth medium containing 50 µM ganciclovir (Sigma-Aldrich). The selection was performed for 10-14 days to get resistant colonies that had undergone RCME. Single-cell sorting into a 96-well plate was performed. Clones were tested for reporter expression using luciferase assays.

***Renilla* luciferase assays**

Reporter production was measured with Promega's *Renilla* Luciferase Assay System. The described cell lines were seeded on 12-well plates. The next day, plasmid DNA was transfected once cells reached approximately 70% confluency as described above. On the subsequent day, the expression of reporters was induced with 1 µg/ml doxycycline (Sigma) for 3 hours unless otherwise specified. Stress was induced by adding 1 mM/ml sodium arsenite (Sigma) for the last 1 hour of induction. To measure recovery, cells were washed twice with

PBS and replaced with fresh culturing medium. At the specified time points, cells were washed once with PBS and lysed with 250 µl Passive Lysis Buffer per well. To ensure full cellular lysis, plates were gently shaken for 15 minutes at room temperature. 30 µl lysate was transferred to 96-well EIA/RIA Plate (Costar) in triplicates. Bioluminescence was measured 2 seconds after injecting 12 µl *Renilla* Luciferase Assay Reagent per well. Measurements were performed on the Mithras Multimode Microplate Reader LB 940 (Berthold). Data were normalized by protein concentration measured by standard Bradford Protein Assay. Means of at least 3 biological replicates (each with 3 described technical replicates) were calculated.

Single-molecule fluorescence in situ hybridization (FISH)

Single-molecule RNA detection against the *Renilla* coding sequence and MS2 (v5) was performed using Stellaris FISH probes (Biosearch Technologies). Probes targeting MS2 (v4) were made by enzymatic oligonucleotide labeling [35] with Amino-11-ddUTP (Lumiprobe) and Atto647-NHS (ATTO-TEC).

Cells were seeded on glass coverslips (Paul Marienfeld GmbH) placed in 12-well plates. The next day, cells were transfected as indicated. On the subsequent day, cells were treated as indicated, followed by two washes with PBS and fixation in 4% paraformaldehyde (Electron Microscopy Sciences) diluted in PBS for 5 minutes. Cells were washed thrice with PBS and permeabilized with 0.5% Triton X-100 diluted in PBS for 5 minutes (if immunofluorescence was performed) or overnight at 4°C in 70% Ethanol. Cells were washed two more times with PBS and prehybridized with wash buffer (2x SSC (Invitrogen), 10% v/v formamide (Abcam)) twice for 5 minutes. Coverslips were then incubated between 4 and 16 hours with hybridization solution (2x SSC, 10% v/v formamide, 10% v/v dextran sulfate, 0.5% v/v BSA, 200 nM FISH probes) at 37°C in humidified chambers. Cells were washed once more with wash buffer for 30 minutes and twice with PBS. Immunofluorescence staining was performed according to the "Immunofluorescence" section from BSA blocking

to mounting. Samples were then mounted on ProLong Gold Antifade Mountant with DAPI. Imaging was performed as described in the "Live-cell imaging" section using sequential, single-camera acquisition.

Immunofluorescence

Cells were seeded on glass coverslips (Paul Marienfeld GmbH) placed in 12-well plates. The next day, cells were transfected as indicated. On the subsequent day, cells were treated as indicated, followed by two washes with PBS and fixation in 4% v/v paraformaldehyde (Electron Microscopy Sciences) diluted in PBS for 5 minutes. Cells were washed thrice with PBS and permeabilized with 0.5% v/v Triton X-100 diluted in PBS for 5 minutes. Cells were washed two more times in PBS and incubated in 3% w/v bovine serum albumin (BSA) (Sigma-Aldrich) diluted in PBS for 1 hour. Primary antibodies (diluted in 1% w/v BSA in PBS) were incubated for 1 hour at room temperature or overnight at 4^{o}C. After washing three times with PBS, the cells were incubated with secondary antibodies (diluted in 1% w/v BSA in PBS) for 1 hour at room temperature. Cells were washed twice with PBS and mounted on glass slides in ProLong Gold Antifade Mountant with DAPI. Imaging was performed as described in the "Live-cell imaging" section using sequential, single-camera acquisition.

Live-cell imaging

Cells were seeded on 35 mm glass-bottom µ-Dish (ibidi GmbH). The next day, cells were transfected as indicated. On the subsequent day, cells were treated as indicated. During the last 15 minutes of treatment, the medium was supplemented with JF585 HaloTag ligand, obtained from L. Lavis (Janelia Research Campus) [24, 25], at 100 nM final concentration. After incubation, cells were washed once with PBS and kept in FluoroBrite DMEM (Life Technologies) containing 10% v/v FBS and 4 mM L-glutamine. Cells were imaged within 15 minutes of medium exchange on an inverted Ti2-E Eclipse microscope (Nikon)

with a CSU-W1 Confocal Scanner Unit (Yokogawa), two back-illuminated EM-CCD cameras iXon-Ultra-888 (Andor), an MS-2000 motorized stage (Applied Scientific Instrumentation), and VisiView imaging software (Visitron Systems GmbH). Specimens were illuminated with 561 Cobolt Jive (Cobolt), 405 iBeam Smart, 488 iBeam Smart, and 639 iBeam Smart lasers (Toptica Photonics) and a VS-Homogenizer (Visitron Systems GmbH). All images were acquired with a CFI Plan Apochromat Lambda 100X Oil/1.45 objective (Nikon). This setup results in a pixel size of 130 nm. Unless otherwise indicated, excitation was performed with a 50 ms exposure time in a single plane. The second camera was used to detect the 488 nm channel. To ensure proper camera alignment, TetraSpeck^{TM} Fluorescent Microspheres Size Kit (Thermo Fisher Scientific) was used to image 0.5 µm fluorescent beads after each imaging session. Cells were maintained at 37°C and 5% CO_2 within an incubation box.

2.3 Quantification and Statistical Analysis

Detection of mRNA spots from smFISH and colocalization

Using custom-built python scripts, images were registered and maximum intensity projected in all channels. Cells were segmented in two steps. First, a sequential workflow comprising Gaussian filtering steps, Otsu thresholding [36], and distance transform calculations of the DAPI channel (405 nm) was used to segment individual nuclei. Subsequently, the nuclei were used as seeds to perform a watershed segmentation into a previously thresholded cytoplasmic map. Cytoplasmic channels were chosen based on their signal uniformity (561 nm *Renilla* or MS2v5 probe channel). SGs were segmented in Fluffy [31]. mRNA spots were detected with a Laplacian of Gaussian. Thresholds for cellular segmentation and spot detection were kept constant throughout a dataset. To colocalize mRNA spots, Euclidean distances were calculated between spots across both channels. To ensure proper channel-to-channel

association of mRNA spots, cells with a high spot density were filtered out. Cellular outliers with significantly higher or lower nuclear areas, cytoplasmic areas or absolute spot numbers were removed. Two mRNAs were considered as colocalized when their coordinates are less than 2 px (240 nm) apart. For TREAT experiments, each spot in the measurement channel should be paired to a spot in the reference channel. Therefore, cells with low measurement-to-reference pairing were excluded from the analysis.

Processing of live-cell imaging data

Images of the fluorescent beads were used to perform channel alignment. Using the pystackreg python package [37] an affine transformation was registered. This model was subsequently re-applied to all images acquired with the secondary camera. Fiji [30] was used to create representative movies and images via cropping, brightness adjustments, channel merging, and scale bar annotation. TrackMate [33] was used to display tracked particles.

Quantification of translational status

Tracking-based quantification of translation was performed using a KNIME [32] workflow described in Mateju et al. [13] in section “Track-based analysis of translational status and colocalization” without including the described SG association component.

Statistics

Results are presented as the mean $\pm$ confidence interval (95%) of independent experiments. Significant differences between variables are based on independent sample t-tests. P-values are indicated using stars in each figure. Each star corresponds to the following p-values:

- ns: $5e^{-2} < p <= 1$
- *: $e^{-2} < p <= 5e^{-2}$
- **: $e^{-3} < p <= e^{-2}$

- ***: $e^{-4} < p <= e^{-3}$
- ****: $p <= e^{-4}$

2.4 Data and Code Availability

The code used to analyze and visualize the data together with plasmid maps is available on GitHub[1]. All data supporting the findings of this study are available on reasonable request.

[1] https://github.com/BBQuercus/master-thesis

3 Results

3.1 G3BP1 tethering affects mRNA dynamics

Proteins of the G3BP RNA-binding family are key components of SGs. In mammals, G3BP1 (and its paralog G3BP2) were reported to be essential in nucleating the formation of SGs [38]. SGs can not only be induced by stress (e.g. sodium arsenite) but also by the overexpression of G3BPs [6]. In addition, a recent imaging-based study Markmiller et al. [39] showed that "many well-characterized SG proteins (e.g., G3BP1, TIA1, CAPRIN1, PABPC1, FMR1, and ATXN2) were identified as highly significant interactors". This finding might suggest the formation of an mRNP complex containing SG proteins allowing for a rapid assembly.

The exact role of G3BPs in SG assembly as well as in unstressed cells is still largely unknown. As reviewed in Alam and Kenedy [40] various functions have been attributed to this protein family. These range from transcript destabilization and repression to the polar opposite in transcript stabilization. Furthermore, G3BP's also showed effects on transcript localization and sequestration to virus-induced foci. The only consensus is G3BP's involvement in mRNA translational control. The subsequent experiments attempt to clarify this disunity by analyzing G3BP1's effect on mRNA transcripts at a single-molecule level. For this reason, I designed an assay to tether G3BP1 and reporter mRNAs together and thereby promoting mRNA accumulation in SGs.

This study focussed on one reporter RNA containing a SunTag cassette, the

gene encoding for *Renilla* luciferase and MS2 stem-loops (Figure 3.1A). These stem-loops are structural motifs derived from phages and can be specifically recognized by a bacteriophage MS2 coat protein (MCP). G3BP1 was fused to MCP (abbreviated as MCPG3) in an attempt to promote mRNA recruitment to SGs. The construct was validated by FISH against the reporter RNA followed by immunofluorescence for the endogenous SG marker TIA-1 [5] (Figure 3.1B). SGs were induced by sodium arsenite treatment (1 mM/ml for 1 hour). As a control, an identical construct only lacking G3BP1 fusion was

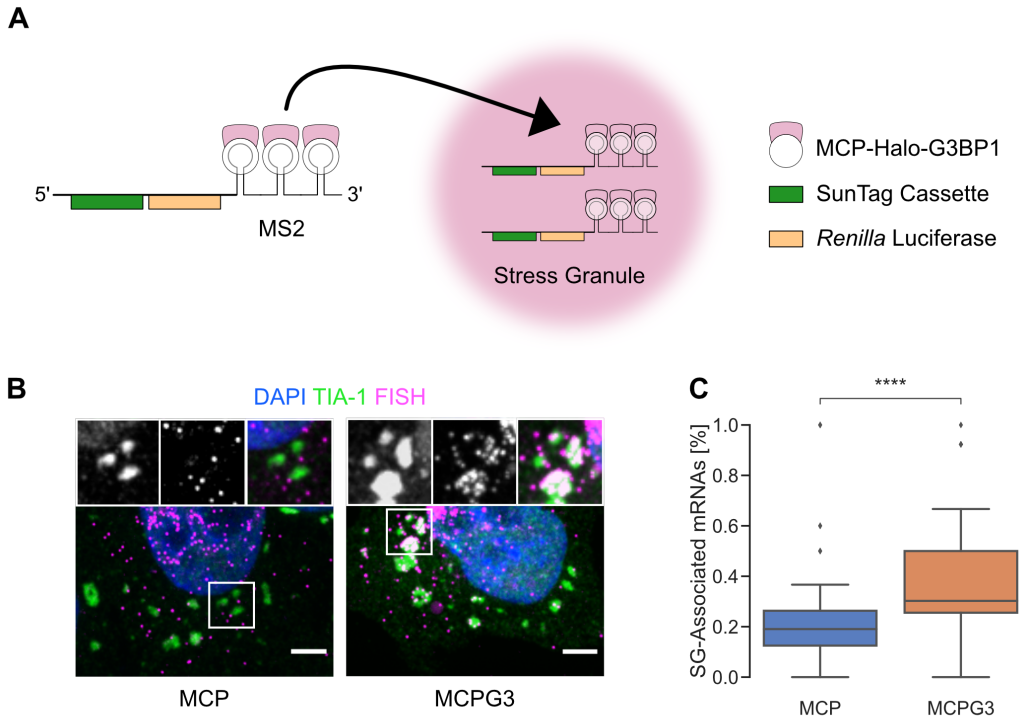

Figure 3.1: Design of MCP-G3BP1. (A) Schematic depiction of MCP-G3BP1 function. (B) Representative fluorescence images of the SG marker TIA-1 and the tethered RNAs. To induce SGs, cells were treated with 1 mM/ml sodium arsenite for 1 hour. Pannels show TIA-1, FISH, Merge respectively. Scale bars, 10 µm. (C) Quantification of the mRNA recruitment to SGs. Number of cells quantified (left to right): 27, 21.

used. Both by visual inspection as well as by mRNA quantification (Figure 3.1C), a significant difference in SG association can be seen. MCPG3 shows an approximately two-fold increase in SG associated mRNAs compared to the control. Taken together, fusing G3BP1 to MCP seems to be a reliable way to recruit functional G3BP1 to the local vicinity of mRNAs and thereby promote localization to SGs.

3.1.1 Reporter expression is impacted by G3BP1

Having proven that G3BP1 can be recruited to mRNAs, I wanted to investigate the effect on translational activity. *Renilla* luciferase assays are used to measure reporter expression on a global level. As G3BP1 was shown to be involved in stress-induced events as well as in unstressed conditions, the luciferase activity at multiple time points in unstressed cells as well as in cells recovering from oxidative stress was measured.

The recruitment of G3BP1 to mRNAs showed a significant increase in luciferase readings when looking at the time-points for induction (Figure 3.2A). This suggests that the presence of G3BP1 might promote protein synthesis. Comparing both constructs during stress recovery, one can observe a slightly less significant but still noticeable increase in luciferase activity for MCPG3 expressing cells (Figure 3.2B). Interestingly, the largest effects are at later time points and during non-stress conditions while not being immediately after stress recovery. This suggests a lesser involvement of G3BP1 on translational activity during stress. SGs have been observed to persist between a few minutes to hours [41]. This correlates with the time when an increase in luciferase activity can be observed again.

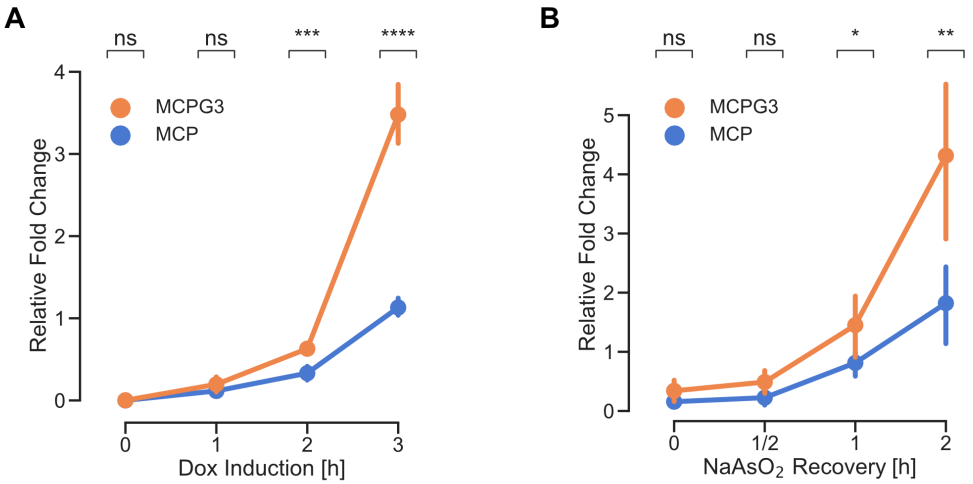

Figure 3.2: G3BP1 tethering increases global translational activity. (A) Luciferase assays at different time points during induction. (B) Sodium arsenite stress recovery time points after induction. Cells were induced for 3 hours and stressed with sodium arsenite (1 mM/ml) in the last hour. Time point capture started immediately after washing out stressor. (A and B) Data normalized to the 3 hour induction condition of MCP.

3.1.2 G3BP1 does not alter mRNA translation

The observed differences in luciferase activity described in Section 3.1.1 can result from various causes. These differences in reporter protein synthesis levels could arise from an increase in translational activity of mRNAs or an increase in mRNA stability. The translation site imaging method SunTag (see Section 1.2) can be used to address this option.

In SunTag, the fluorescence intensity is a direct measure of translation rate. Therefore, to analyze the translation activity of MCPG3-bound mRNAs, the track intensity was quantified. Track intensity refers to the average fluorescence intensity over the entire track duration.

During stress conditions, most mRNAs get translationally silenced (reviewed in Holcik and Sonenberg [42]). To image translation sites despite this silencing,

images were acquired 15 to 30 minutes after removing the stressor.

Image-level SunTag track intensities in cells expressing MCPG3 or control MCP (Figure 3.3A). Both conditions show similar fluorescence intensities suggesting G3BP1 does not have a major effect on mRNA translation rates. The lower readings of fluorescent intensity in the stress condition can be explained by translational silencing during stress which was not fully recovered. Similarly, the grouping of SunTag tracks into segmented cells shows comparable mean intensities in cells expressing MCPG3 or control MCP. Equivalently to the image-level analysis, cellular intensities (Figure 3.3B) do not yield different results. Similarly, the average intensity of all tracks per cell does not appear to be affected by G3BP1 fusion.

Lastly, global translation can also increase by a higher number of translating transcripts per cell. However, as is evident from Figure 3.3C the number of tracks stays consistent in all experiments. This suggests that G3BP1 does not have a profound impact on translation activity.

Figure 3.3: Transcript level imaging of mRNAs. (A) Distribution of the mean fluorescence intensity of tracked mRNAs in the full-sized image (without cellular segmentation). The total number of tracks (left to right): 715, 1064, 997, 3442. (B) Track intensity averaged per cell. (A and B) Data normalized to the Dox induction condition for MCP. (C) The number of tracks registered per cell. (B and C) The total number of cells (left to right): 48, 77, 31, 48.

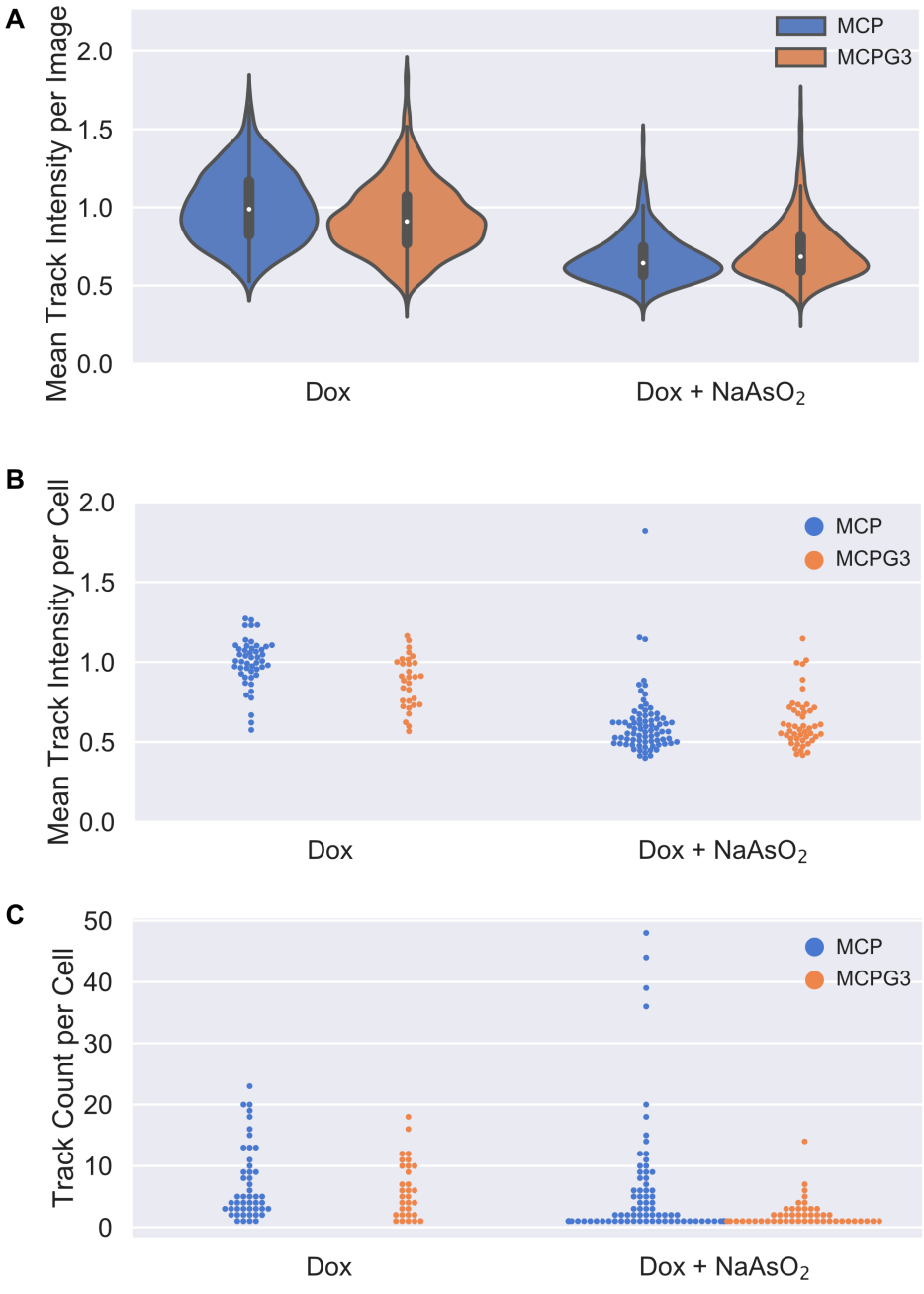

Figure 3.3: (On the previous page.)

3.1.3 Transcript stability is affected by G3BP1 tethering

SunTag measurements (see Section 3.1.2) did not suggest any effect of G3BP1 on translational activity. Alternatively, a decrease in mRNA degradation could also explain the original luciferase readings. To ask whether G3BP1 has an mRNA stabilizing effect, I compared the number of intact transcripts between MCPG3 and the control using 3(three)'-RNA end accumulation during turnover (TREAT) [29].

TREAT uses a slightly modified reporter mRNA containing viral RNA pseudoknot (PK) structures upstream of the MS2 stem-loops. These PKs can block Xrn1 mediated 5'-3' degradation of a transcript by sequestering the 5' phosphate group [43]. Subsequently, by using FISH probes against *Renilla* luciferase upstream of PKs (showing intact mRNAs) and FISH probes against MS2 stem-loops downstream of PKs (showing both intact and degraded mRNAs) one can quantify the number of intact transcripts.

To look at transcript stabilization, a cell line expressing the aforementioned TREAT mRNA reporter was used. Five time points were chosen after a 1 hour induction followed by thorough washing to halt any further transcription. As can be seen in Figure 3.4A, transcripts get exported to the cytosol as soon as transcription is stopped.

When comparing the percentage of intact mRNAs, i.e. transcripts still containing FISH spots against both *Renilla* luciferase and MS2, between MCPG3 and the control, a striking difference is evident (Figure 3.4B). The G3BP1 fusion shows a significant reduction in degraded transcripts compared to the control suggesting an increase in mRNA stability. This effect is not reflected in the mRNA count from the SunTag measurements (see Section 3.1.2) which might arise from the nature of the SunTag cassette that will be discussed in the following Section 3.2.

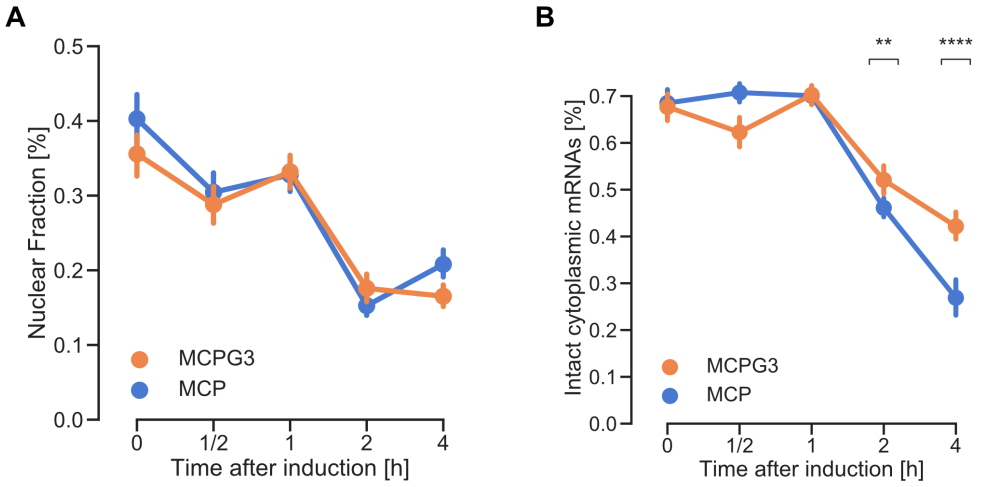

Figure 3.4: TREAT based mRNA stability assay. (A) The fraction of nuclear mRNAs (of total cellular mRNAs) at different time points after induction. (B) Percentage of intact cytoplasmic mRNAs at different time points. (A and B) Number of cells quantified (ascending, MCP then MCPG3): 117, 154, 200, 175, 55, 114, 148, 167, 111, 132.

3.2 How can the SunTag reporter be improved?

The original design of the SunTag cassette consists of 24 GCN4 repeats. These completely disordered repeats are thought to aggregate and could lead to a decrease in translation rates [44]. In an attempt to decrease protein disorder, a spaghetti monster reporter was made [45]. Spaghetti monster green fluorescent proteins (smGFP) are essentially a non-fluorescent green fluorescent protein's (GFP) beta-barrel used to attach small epitope tags. Here, three GCN4 repeats each were placed at the N-terminus, C-terminus, and 10/11-loop of the GFP beta-barrel as shown in Figure 3.5A. Previously, other tags, such as influenza hemagglutinin (HA), were used and visualized with frankenbodies (single-chain antibodies targeting various tags). In this study, I attempt to combine SunTag imaging with smGFP constructs.

Initially, it was of interest to see whether the smGFP reporter has higher

translational activity. As is evident from Figure 3.5B, the new reporter shows an approximative 4-fold increase in luciferase activity compared to the original SunTag reporter. A pure *Renilla* reporter was used as control which does not contain any GCN4 repeats. While the smGFP reporter drastically increases activity, it does not yet reach the levels of the control. It must be noted, that the control construct does not contain an FKBP tag which has lowered the luciferase activity in previous experiments by enhancing the degradation of the tagged protein [46].

To look at the effect of the new reporter in live cells, stable cell lines were created and observed after 1 hour of induction. From a representative image in Figure 3.5C, one can see that cells typically have more, slightly dimmer translation sites. Quantification of images showed a significant increase in the number of translation sites per cell compared to the cells expressing the standard SunTag reporter (Figure 3.5D). The brightness of individual spots decreased around 2.7 fold (Figure 3.5E). This decrease can be explained by a lower number of GCN4 repeats available for the scAB to bind. Whereas the standard SunTag has 24 GCN4 repeats, smGFP only has 9 leading to a binding site difference of $2.6\overline{6}$ to 1.

Taken together, this study proposes a new SunTag reporter which increases translational activity by greatly increasing the number of active transcription sites. This new reporter allows for shorter induction times and the folded structure should reduce aggregation-based problems.

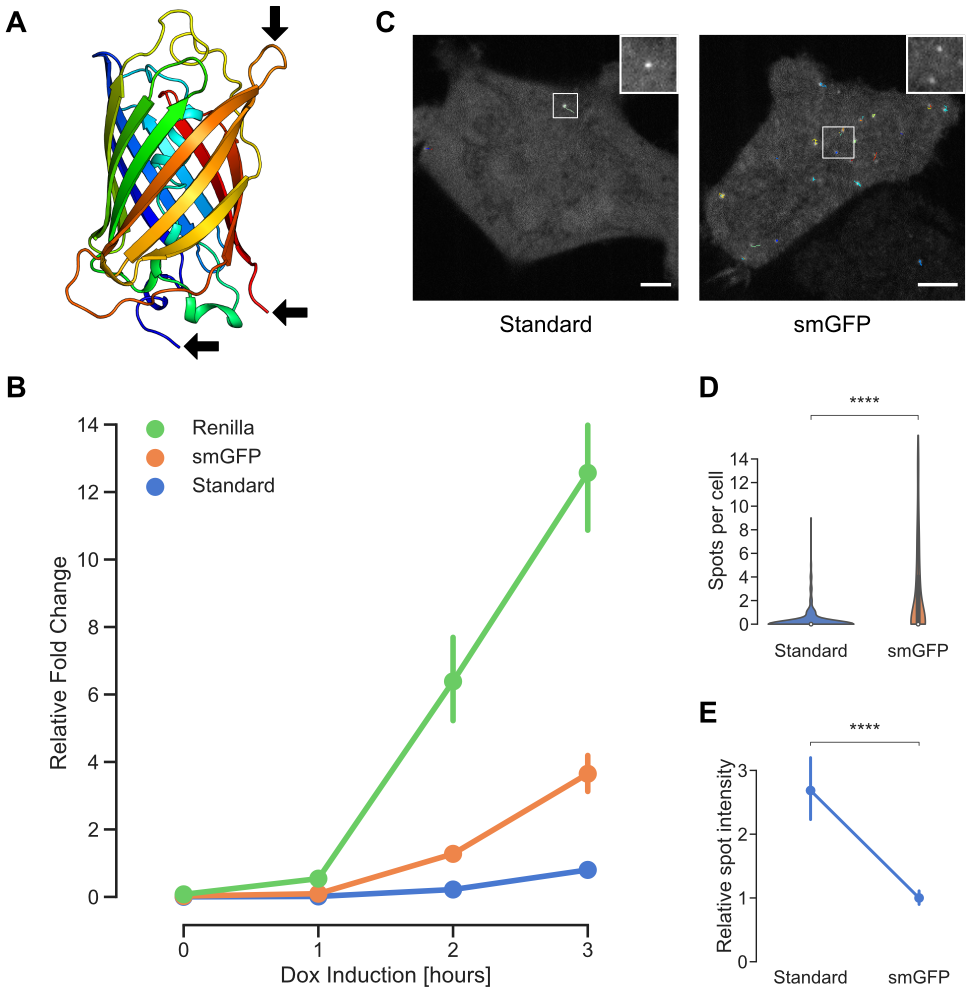

Figure 3.5: Overview of the smGFP SunTag reporter. (A) Structural overview of GCN4 repeat placement on the smGFP beta-barrel (PDB ID: 1GFL [47]). (B) Relative luciferase activity comparing the standard SunTag reporter, the smGFP SunTag reporter, and a Renilla reporter without SunTag cassette. (C) Representative fluorescence images. Each recorded mRNA track is visualized with a unique color. Scale bar, 10 µm. The inset shows spots from raw images without brightness corrections. (D) Quantification of translation site count per cell. The number of cells quantified (left to right): 286, 233. (E) Average spot intensity normalized to the smGFP reporter. The number of spots quantified (left to right): 36, 39.

4
Discussion

The role of SG-proteins in unstressed cells is still unclear. An understanding of these proteins, such as G3BP1 could provide important insights into how SGs form and what functional purpose they serve. This study approaches this mystery experimentally.

Fusing G3BP1 to MCP has profound effects on their attached mRNAs. First, mRNAs are more likely to get recruited to SGs. The nature of transient transfections used for these sets of experiments likely lowered the number measured if all cells were expressing the construct. Furthermore, due to highly clustered mRNAs in SGs accurate quantification was proven to be rather difficult also decreasing the number. Second, G3BP1 has a significant effect on protein expression irrespective of cellular stress. This interesting finding showed that the role of G3BP1 in SGs might just be secondary while it's more important function occurs in normal cell homeostasis. As previously proposed, SGs might arise from the necessity to sequester proteins like G3BP1 from mRNA targets in the cytosol [48]. SunTag imaging experiments were performed to observe differences in translational activity. These, however, were inconclusive and no major differences occurred suggesting that G3BP1 might only have minor roles in translational initiation or elongation. Surprisingly, TREAT assays looking at mRNA stability showed significant differences. This suggests that G3BP1 might actively reduce 5'-3' degradation by sequestering RNase binding sites or inhibiting RNases altogether. Taken together, while some recent publications assume a decay promoting role of G3BP1 [48, 49], others including this study have suggested the opposite [50, 51, 52]. The role

of G3BP1 in mRNA metabolism remains debated and needs further clarification on a molecular level.

In an effort to reduce the aggregation potential of the currently used SunTag reporter cassette, a novel cassette relying on the structural support by smGFP was created. The preliminary results shown here suggest that binding affinities are comparable with the previous version while greatly increasing translational activity. This seems to mainly be achieved through more translating transcripts per cell. The lower signal intensity has shown to make a track based analysis slightly harder. To counteract this, one could, however, use two or more cassettes or add more repeats at other locations within the structural scaffold. Looking forward, it would be interesting to see if mRNA stability is also affected and how the system can be evolved. Recent progress in single-chain antibodies leads the way to a highly interchangeable system with different tags and fluorescent colors.

Bibliography

[1] Melissa J. Moore. From birth to death: the complex lives of eukaryotic mRNAs. *Science (New York, N.Y.)*, 309(5740):1514–1518, September 2005.

[2] Paul Anderson and Nancy Kedersha. RNA granules. *The Journal of Cell Biology*, 172(6):803–808, March 2006.

[3] Karolina Pakos-Zebrucka, Izabela Koryga, Katarzyna Mnich, Mila Ljujic, Afshin Samali, and Adrienne M. Gorman. The integrated stress response. *EMBO reports*, 17(10):1374–1395, October 2016.

[4] Scot R. Kimball, Rick L. Horetsky, David Ron, Leonard S. Jefferson, and Heather P. Harding. Mammalian stress granules represent sites of accumulation of stalled translation initiation complexes. *American Journal of Physiology. Cell Physiology*, 284(2):C273–284, February 2003.

[5] Nancy L. Kedersha, Mita Gupta, Wei Li, Ira Miller, and Paul Anderson. RNA-Binding Proteins Tia-1 and Tiar Link the Phosphorylation of Eif-2α to the Assembly of Mammalian Stress Granules. *The Journal of Cell Biology*, 147(7):1431–1442, December 1999.

[6] Helene Tourrière, Karim Chebli, Latifa Zekri, Brice Courselaud, Jean Marie Blanchard, Edouard Bertrand, and Jamal Tazi. The RasGAP-associated endoribonuclease G3BP assembles stress granules. *The Journal of Cell Biology*, 160(6):823–831, March 2003.

[7] Natalie Gilks, Nancy Kedersha, Maranatha Ayodele, Lily Shen, Georg Stoecklin, Laura M. Dember, and Paul Anderson. Stress granule assembly is mediated by prion-like aggregation of TIA-1. *Molecular Biology of the Cell*, 15(12):5383–5398, December 2004.

[8] Jenifer E. Shattuck, Kacy R. Paul, Sean M. Cascarina, and Eric D. Ross. The prion-like protein kinase Sky1 is required for efficient stress granule disassembly. *Nature Communications*, 10(1):1–11, August 2019. Number: 1 Publisher: Nature Publishing Group.

[9] J. Ross Buchan, Denise Muhlrad, and Roy Parker. P bodies promote stress granule assembly in Saccharomyces cerevisiae. *The Journal of Cell Biology*, 183(3):441–455, November 2008.

[10] Pavel A Ivanov, Elena M Chudinova, and Elena S Nadezhdina. Disruption of microtubules inhibits cytoplasmic ribonucleoprotein stress granule formation. *Experimental Cell Research*, 290(2):227–233, November 2003.

[11] J. Ross Buchan and Roy Parker. Eukaryotic Stress Granules: The Ins and Outs of Translation. *Molecular Cell*, 36(6):932–941, December 2009.

[12] María Gabriela Thomas, Mariela Loschi, María Andrea Desbats, and Graciela Lidia Boccaccio. RNA granules: the good, the bad and the ugly. *Cellular signalling*, 23(2):324–334, February 2011.

[13] Daniel Mateju, Bastian Eichenberger, Jan Eglinger, Gregory Roth, and Jeffrey Chao. Single-molecule imaging reveals translation of mRNAs localized to stress granules. *bioRxiv*, page 2020.03.31.018093, April 2020. Publisher: Cold Spring Harbor Laboratory Section: New Results.

[14] Vladimir I. Bashkirov, Harry Scherthan, Jachen A. Solinger, Jean-Marie Buerstedde, and Wolf-Dietrich Heyer. A Mouse Cytoplasmic Exoribonuclease (mXRN1p) with Preference for G4 Tetraplex Substrates. *Journal of Cell Biology*, 136(4):761–773, February 1997. Publisher: The Rockefeller University Press.

[15] Roy Parker and Ujwal Sheth. P bodies and the control of mRNA translation and degradation. *Molecular Cell*, 25(5):635–646, March 2007.

[16] Ujwal Sheth and Roy Parker. Decapping and Decay of Messenger RNA Occur in Cytoplasmic Processing Bodies. *Science (New York, N.Y.)*, 300(5620):805–808, May 2003.

[17] Marvin E. Tanenbaum, Luke A. Gilbert, Lei S. Qi, Jonathan S. Weissman, and Ronald D. Vale. A Protein-Tagging System for Signal Amplification in Gene Expression and Fluorescence Imaging. *Cell*, 159(3):635–646, October 2014.

[18] Logan George, Fred E. Indig, Kotb Abdelmohsen, and Myriam Gorospe. Intracellular RNA-tracking methods. *Open Biology*, 8(10), October 2018.

[19] Christian Genz, Julia Fundakowski, Orit Hermesh, Maria Schmid, and Ralf-Peter Jansen. Association of the Yeast RNA-binding Protein She2p with the Tubular Endoplasmic Reticulum Depends on Membrane Curvature. *The Journal of Biological Chemistry*, 288(45):32384–32393, November 2013.

[20] Tomas J. Bos, Julia K. Nussbacher, Stefan Aigner, and Gene W. Yeo. Tethered Function Assays as Tools to Elucidate the Molecular Roles of RNA-Binding Proteins. *Advances in experimental medicine and biology*, 907:61–88, 2016.

[21] Na Yeon Kim, Sangkyu Lee, Jeonghye Yu, Nury Kim, Seong Su Won, Hyerim Park, and Won Do Heo. Optogenetic control of mRNA localization and translation in live cells. *Nature Cell Biology*, 22(3):341–352, March 2020. Number: 3 Publisher: Nature Publishing Group.

[22] Mauro Ferreira de Azevedo, Paul R. Gilson, Heloisa B. Gabriel, Roseli F. Simões, Fiona Angrisano, Jacob Baum, Brendan S. Crabb, and Gerhard Wunderlich. Systematic Analysis of FKBP Inducible Degradation Domain Tagging Strategies for the Human Malaria Parasite Plasmodium falciparum. *PLOS ONE*, 7(7):e40981, July 2012. Publisher: Public Library of Science.

[23] Ina Weidenfeld, Manfred Gossen, Rainer Löw, David Kentner, Stefan Berger, Dirk Görlich, Dusan Bartsch, Hermann Bujard, and Kai Schönig. Inducible expression of coding and inhibitory RNAs from retargetable genomic loci. *Nucleic Acids Research*, 37(7):e50–e50, April 2009. Publisher: Oxford Academic.

[24] Jonathan B. Grimm, Brian P. English, Jiji Chen, Joel P. Slaughter, Zhengjian Zhang, Andrey Revyakin, Ronak Patel, John J. Macklin, Davide Normanno, Robert H. Singer, Timothée Lionnet, and Luke D. Lavis. A general method to improve fluorophores for live-cell and single-molecule microscopy. *Nature Methods*, 12(3):244–250, 3 p following 250, March 2015.

[25] Jonathan B. Grimm, Anand K. Muthusamy, Yajie Liang, Timothy A. Brown, William C. Lemon, Ronak Patel, Rongwen Lu, John J. Macklin, Philipp J. Keller, Na Ji, and Luke D. Lavis. A general method to fine-tune fluorophores for live-cell and in vivo imaging. *Nature Methods*, 14(10):987–994, October 2017.

[26] Johannes H. Wilbertz, Franka Voigt, Ivana Horvathova, Gregory Roth, Yinxiu Zhan, and Jeffrey A. Chao. Single-Molecule Imaging of mRNA Localization and Regulation during the Integrated Stress Response. *Molecular Cell*, 73(5):946–958.e7, 2019.

[27] Franka Voigt, Hui Zhang, Xianying A. Cui, Désirée Triebold, Ai Xin Liu, Jan Eglinger, Eliza S. Lee, Jeffrey A. Chao, and Alexander F. Palazzo. Single-Molecule Quantification of Translation-Dependent Association of mRNAs with the Endoplasmic Reticulum. *Cell Reports*, 21(13):3740–3753, December 2017.

[28] Caroline Beard, Konrad Hochedlinger, Kathrin Plath, Anton Wutz, and Rudolf Jaenisch. Efficient method to generate single-copy transgenic

mice by site-specific integration in embryonic stem cells. *Genesis (New York, N.Y.: 2000)*, 44(1):23–28, January 2006.

[29] Ivana Horvathova, Franka Voigt, Anna V. Kotrys, Yinxiu Zhan, Caroline G. Artus-Revel, Jan Eglinger, Michael B. Stadler, Luca Giorgetti, and Jeffrey A. Chao. The Dynamics of mRNA Turnover Revealed by Single-Molecule Imaging in Single Cells. *Molecular Cell*, 68(3):615–625.e9, November 2017.

[30] Johannes Schindelin, Ignacio Arganda-Carreras, Erwin Frise, Verena Kaynig, Mark Longair, Tobias Pietzsch, Stephan Preibisch, Curtis Rueden, Stephan Saalfeld, Benjamin Schmid, Jean-Yves Tinevez, Daniel James White, Volker Hartenstein, Kevin Eliceiri, Pavel Tomancak, and Albert Cardona. Fiji: an open-source platform for biological-image analysis. *Nature Methods*, 9(7):676–682, June 2012.

[31] Bastian Eichenberger. Fluffy – reproducible deep learning based segmentation of biomedical images., March 2020.

[32] Michael R. Berthold, Nicolas Cebron, Fabian Dill, Thomas R. Gabriel, Tobias Kötter, Thorsten Meinl, Peter Ohl, Kilian Thiel, and Bernd Wiswedel. KNIME - the Konstanz information miner: version 2.0 and beyond, November 2009.

[33] Jean-Yves Tinevez, Nick Perry, Johannes Schindelin, Genevieve M. Hoopes, Gregory D. Reynolds, Emmanuel Laplantine, Sebastian Y. Bednarek, Spencer L. Shorte, and Kevin W. Eliceiri. TrackMate: An open and extensible platform for single-particle tracking. *Methods (San Diego, Calif.)*, 115:80–90, 2017.

[34] Daniel G. Gibson, Lei Young, Ray-Yuan Chuang, J. Craig Venter, Clyde A. Hutchison, and Hamilton O. Smith. Enzymatic assembly of DNA molecules up to several hundred kilobases. *Nature Methods*, 6(5):343–345, May 2009.

[35] Imre Gaspar, editor. *RNA Detection: Methods and Protocols*. Methods in Molecular Biology. Humana Press, 2018.

[36] Nobuyuki Otsu. A Threshold Selection Method from Gray-Level Histograms. *IEEE Transactions on Systems, Man, and Cybernetics*, 9(1):62–66, January 1979.

[37] P. Thévenaz, U. E. Ruttimann, and M. Unser. A pyramid approach to subpixel registration based on intensity. *IEEE transactions on image processing: a publication of the IEEE Signal Processing Society*, 7(1):27–41, 1998.

[38] Nancy Kedersha, Marc D. Panas, Christopher A. Achorn, Shawn Lyons, Sarah Tisdale, Tyler Hickman, Marshall Thomas, Judy Lieberman, Gerald M. McInerney, Pavel Ivanov, and Paul Anderson. G3BP-Caprin1-USP10 complexes mediate stress granule condensation and associate with 40S subunits. *The Journal of Cell Biology*, 212(7):845–860, March 2016.

[39] Sebastian Markmiller, Sahar Soltanieh, Kari L. Server, Raymond Mak, Wenhao Jin, Mark Y. Fang, En-Ching Luo, Florian Krach, Dejun Yang, Anindya Sen, Amit Fulzele, Jacob M. Wozniak, David J. Gonzalez, Mark W. Kankel, Fen-Biao Gao, Eric J. Bennett, Eric Lécuyer, and Gene W. Yeo. Context-Dependent and Disease-Specific Diversity in Protein Interactions within Stress Granules. *Cell*, 172(3):590–604.e13, January 2018.

[40] Umber Alam and Derek Kennedy. Rasputin a decade on and more promiscuous than ever? A review of G3BPs. *Biochimica Et Biophysica Acta. Molecular Cell Research*, 1866(3):360–370, 2019.

[41] Lihua Chen and Beidong Liu. Relationships between Stress Granules, Oxidative Stress, and Neurodegenerative Diseases. *Oxidative Medicine and Cellular Longevity*, 2017, 2017.

[42] Martin Holcik and Nahum Sonenberg. Translational control in stress and apoptosis. *Nature Reviews. Molecular Cell Biology*, 6(4):318–327, April 2005.

[43] Jeffrey S. Kieft, Jennifer L. Rabe, and Erich G. Chapman. New hypotheses derived from the structure of a flaviviral Xrn1-resistant RNA: Conservation, folding, and host adaptation. *RNA biology*, 12(11):1169–1177, 2015.

[44] Thomas Gurry. *Order, disorder, and protein aggregation*. Thesis, Massachusetts Institute of Technology, 2015. Accepted: 2015-06-10T19:12:13Z.

[45] Ning Zhao, Kouta Kamijo, Philip D. Fox, Haruka Oda, Tatsuya Morisaki, Yuko Sato, Hiroshi Kimura, and Timothy J. Stasevich. A genetically encoded probe for imaging nascent and mature HA-tagged proteins in vivo. *Nature Communications*, 10(1):1–16, July 2019. Number: 1 Publisher: Nature Publishing Group.

[46] Kimberly M. Bonger, Ling-chun Chen, Corey W. Liu, and Thomas J. Wandless. Small molecule displacement of a cryptic degron causes conditional protein degradation. *Nature chemical biology*, 7(8):531–537, July 2011.

[47] F. Yang, L. G. Moss, and G. N. Phillips. The molecular structure of green fluorescent protein. *Nature Biotechnology*, 14(10):1246–1251, October 1996.

[48] Joseph W. Fischer, Veronica F. Busa, Yue Shao, and Anthony K. L. Leung. Structure-Mediated RNA Decay by UPF1 and G3BP1. *Molecular Cell*, 0(0), February 2020. Publisher: Elsevier.

[49] Hélène Tourrière, Imed-eddine Gallouzi, Karim Chebli, Jean Paul Capony, John Mouaikel, Peter van der Geer, and Jamal Tazi. RasGAP-

Associated Endoribonuclease G3BP: Selective RNA Degradation and Phosphorylation-Dependent Localization. *Molecular and Cellular Biology*, 21(22):7747–7760, November 2001.

[50] Anaïs Aulas, Guillaume Caron, Christos G. Gkogkas, Nguyen-Vi Mohamed, Laurie Destroismaisons, Nahum Sonenberg, Nicole Leclerc, J. Alex Parker, and Christine Vande Velde. G3BP1 promotes stress-induced RNA granule interactions to preserve polyadenylated mRNA. *The Journal of Cell Biology*, 209(1):73–84, April 2015.

[51] Nadine Bley, Marcell Lederer, Birgit Pfalz, Claudia Reinke, Tommy Fuchs, Markus Glaß, Birgit Möller, and Stefan Hüttelmaier. Stress granules are dispensable for mRNA stabilization during cellular stress. *Nucleic Acids Research*, 43(4):e26, February 2015.

[52] John D. Laver, Jimmy Ly, Allison K. Winn, Angelo Karaiskakis, Sichun Lin, Kun Nie, Giulia Benic, Nima Jaberi-Lashkari, Wen Xi Cao, Alireza Khademi, J. Timothy Westwood, Sachdev S. Sidhu, Quaid Morris, Stephane Angers, Craig A. Smibert, and Howard D. Lipshitz. The RNA-Binding Protein Rasputin/G3BP Enhances the Stability and Translation of Its Target mRNAs. *Cell Reports*, 30(10):3353–3367.e7, March 2020.

A

Supplementary Methods

NLS-stdMCP-stdHalo-G3BP1 cloning primers:

- gattaggatctatcgatttactgccgtggcgcaagccccc
- aagttctgtttcagggcccgatggtgatggagaagcctagtcccct
- ctaggcttctccatcaccatcgggccctgaaacagaactt
- gggggcttgcgccacggcagtaaatcgatagatcctaatcaacctc

smGCN4-Renilla-MS2v5 cloning primers:

- tacacgcggccgcaatcatcggtccgggtggatctggaggtggaggttctggaggagaaga
- cctctttccgagccagttcttccctggcccttattccggtttt

Renilla luciferase FISH probes:

- tcgtacaccttggaagccat
- agtgatcatgcgtttgcgtt
- gttcatttgcttgcagcgag
- agttgatgaaggagtccagc
- gcgtgcttctcggaatcata
- cagcgttaccatgcagaaaa
- tcgatgtgaggcacgacgtg
- gatgatgcatctagccacgg
- ttacccattccgatcagatc
- gatccaggaggcgatatgag
- caagcggtgaggtacttgta
- tttggaaggttcagcagctc

- gtggcccacaaagatgattt
- gagtagtgaaaggccagaca
- ttgatcttgtcttggtgctc
- cactctcagcatggacgatg
- caggactcgatcacgtccac
- atatcctcctcgatgtcagg
- ctcttcgctcttgatcaggg
- attctcaagcaccattttct
- gcatggtctcgacgaagaag
- tttccgcatgatcttgcttg
- cttgaatggctccaggtagg
- gagagggtaggccgtctaac
- ttaacgagagggatctcgcg
- gacaatctggacgacgtcgg
- gaaggtaggcgttgtagttg
- gaacatcttaggcagatcgt
- tggaaaagaacccagggtcg
- cttagctccctcgacaatag
- ttcacgaactcggtgttagg
- cttacccatttcatctggag
- gctccacgaagctcttgatg
- tactgctcgttcttcagcac

MS2v4 FISH probes:

- tgccgtttgtaggtaggatc
- cgcttgaagattggacagtg
- gactgtaatgacagtggagc
- ctgatgctgctggagtttga
- atgtcctgatgtagtcggag
- atcgtcgagcgttgaatgat
- atagtgtctgaggcatgctg
- gtgatcgtgcagccgtttga

- cgataacgtagaggcagtag
- ctgatgctcgtcgcagaaga
- atctggtatgtccgatgttg

MS2v5 FISH probes:

- tgattgtgaagtgtcgggtg
- tccacccttgtgtattgtac
- ctgtgtaatgtgtctggagg
- gtgcttctgtttgattggat
- aaatttggtagcagaagccc
- ccttgttgtagttttttgag
- cagggaatccctgatggtga
- ccctcgtttgacgtatattg
- gatattcgggaggcgtgatc
- acgcactgaattcgaaagcc
- attcgactctgattggctgc
- ctcttcgcgaaagtcgactt
- taagaatggcgcgaaggctg
- gtaggggagagtgtggtttg
- caggaacgctgatgctgttc
- ttttcttgagttgggtactg
- tgatgctgcatggggacata
- ttggggatgtattcttgggg
- ttggtgctcggatgtgattt
- aagaaacaacactccgagcc
- atggagggtttgtccagttg
- tttgtcttgttggtgagagt
- ctgatgctgcttcgagaaga
- gtatgctcgagtgtttcgaa
- gatcgtccacccaagaaata
- aattcgtgagagcatgggtg
- tcgtattggacgtggaacga

- tcgtgatcccgaaaggtaag
- agtggaagtgatgtagctgc
- atcgtgcatgcttgaatgtc
- gttgagacttgtggagcatg
- tgaacccatttggtagtttc
- tttgaggtaggagtgggttc
- ttgccagttttgtgggaaga
- tttggtatgttggaatgggc
- gatgctgtaccagtaattgt
- tagtagtgagagatgtgggc
- tgctgaacggtttggttttt
- ttgatttttccgtgtgtacc
- gtctttcgtatttgtaaacc
- ttgcgctggacgaaagcgtg
- ccgtcggatgtttttcgtaa
- cgtttgtcgtgtttttgtga
- ggttgtaagtttgtgggttg
- ctgaggtgtttgatgtacgg

B

Supplementary Figures

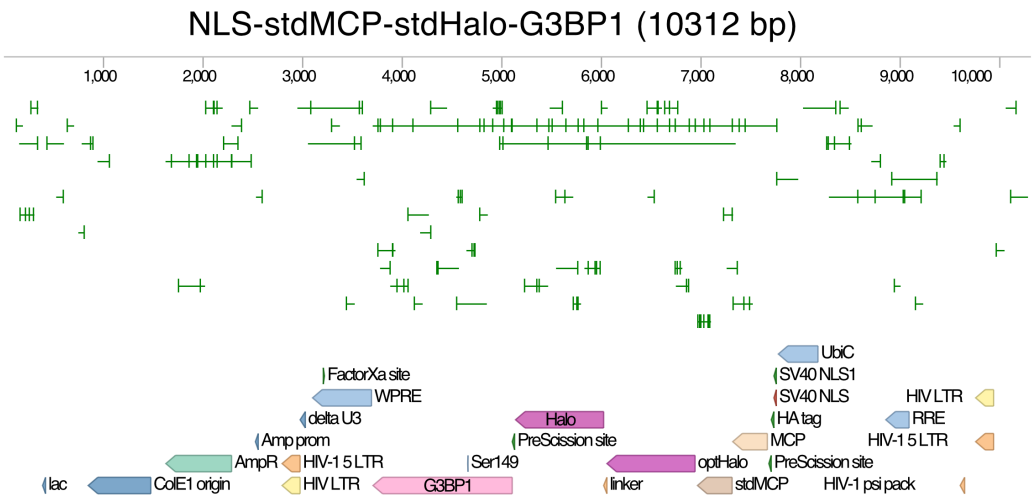

Figure B.1: Design of MCPG3.

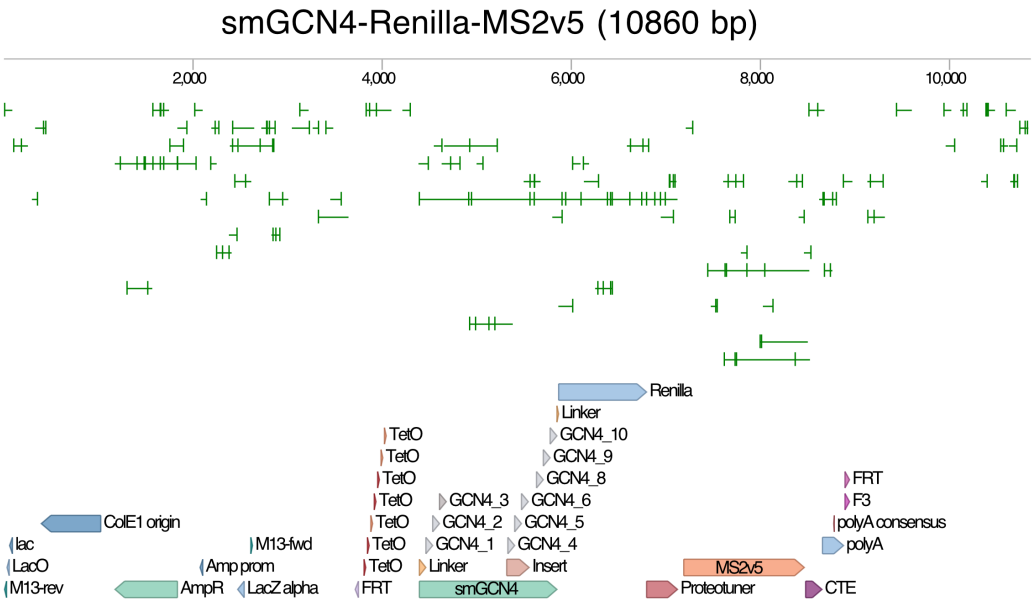

Figure B.2: Design of smGFP SunTag.

Colophon

This document was created using LaTeX and BibTeX typesetting originally developed by Leslie Lamport, based on TeX created by Donald Knuth.
Theme adapted from a design by Tony Beltramelli.
Edited in Visual Studio Code.
The text is set in Helvetica.